Robotica (2015) volume 33, pp. 2156–2165. © Cambridge University Press 2014
doi:10.1017/S0263574714001313

A research on the mounted configuration of end-effector for robotic drilling

Jie Liang*

School of Mechanical Engineering, Zhengzhou University, Zhengzhou 450001, China

(Accepted April 29, 2014. First published online: May 28, 2014)

SUMMARY
The flexible robotic drilling system has been widely used in the aircraft industry in recent years. There are three ways to attach an end-effector to a robot, which are the pointing configuration, the hanging configuration, and the side configuration. The simulation model of robot and workpiece is constructed by using MATLAB software. According to the three configurations, reachability, manipulability, joint useability, and joint passive torque of a robot are calculated by means of the MATLAB language. Based on the calculation results and various measures, the performance, including reachability, manipulability, joint useability, and deformation, of a robot are analyzed. The analysis results show that the pointing configuration has the best reachability, a long service life, and small energy consumption, and it substantially reduces the fifth axis joint passive torque produced by the clamp force, which will improve positional accuracy of holes; the hanging configuration and the side configuration improve robot's manipulability and are suitable for drilling in the curved surface.

KEYWORDS: End-effector; Mounted configuration; Reachability; Manipulability; Joint useability; Joint passive torque.

1. Introduction

The fast development of robotic technology and continuous reduction in robot cost have made robot an effective motion platform, and a robotic drilling system can be created by coupling with a drill end-effector and other sub-systems. The lean system caters for high performance expectations and low cost demands, and it is particularly suited for aerospace assembly. For example, the Electroimpact ONCE system was developed to drill, countersink, and measure fastener holes in the wing trailing edge flaps of Boeing F/A-18E/F Super Hornet.[1] Hawker de Havilland used the 737 aileron robot cell to drill and countersink as well as trim the trailing edge and tooling lugs from the carbon fiber-reinforced plastic skins.[2] The second generation of Electroimpact's ONCE robotic drilling system[3] strove toward "one-up" assembly, whereby the product was assembled for one time – drilled, countersink, inspected, and ultimately fastened – without removal of components for deburring, cleaning, sealing, etc.[4] In order to solve the problems of low efficiency and poor quality in manual drilling of the lower panel of fuel tank, Beijing University of Aeronautics and Astronautics and AVIC Shenyang Aircraft Corporation developed a robotic drilling system that is capable to weld mark inspection, one-sided clamping, real-time thrust force feedback, drilling, and reaming hole in material stack combinations of titanium and aluminium.[5] Webb *et al.*[6] from the University of Nottingham developed a flexible robotic assembly cell, which was designed to be able to both assemble and rivet all the major components required to produce an aircraft fuselage panel.

The above-mentioned robotic drilling systems have three different ways to attach end-effector to a robot, which are the pointing configuration, the hanging configuration, and the side configuration, as shown in Fig. 1. In this study, we analyze the effects of a mounted configuration of an end-effector on reachability, manipulability, joint useability, and joint passive torque of an industrial robot.

The work is presented in the following manner. In Section 2, the robot simulation model is built and the mathematical model is explained. In Section 3, the reachability, manipulability, joint useability,

* E-mail: liangjie812@163.com

https://doi.org/10.1017/S0263574714001313 Published online by Cambridge University Press

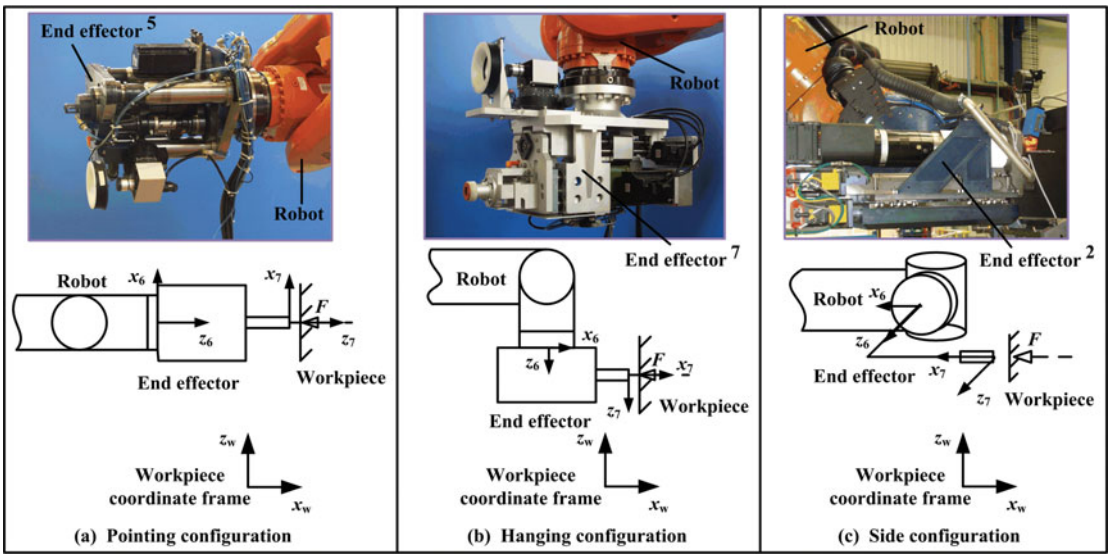


Fig. 1. Mounting configuration of end-effector.

Table I. The Denavit–Hartenberg parameters.

Link	α_i (°)	a_i (m)	d_i (m)	θ_i (°)
1	90	0.32	0.78	−170 170
2	0	1.075	0	−65 85
3	90	0.2	0	−180 70
4	−90	0	1.142	−300 300
5	90	0	0	−120 120
6	0	0	0.2	−360 360

and joint passive torque of a robot are analyzed in different mounted configurations by using the robot simulation model and the mathematical model presented in Section 2. Section 4 describes the implementation of the pointing configuration on the drilling of a titanium panel and presents the results. Conclusions are drawn in Section 5.

2. The Simulation and Mathematical Models

The workpiece is a piece of titanium plate (2.4 × 2.4 × 0.006 m), which is located on the central wing of an aircraft. According to robotic payload, accuracy, repeatability, and price, we choose the ABB IRB6640–235/2.55 industrial robot as a motion platform. The robot's Denavit–Hartenberg parameters and working range are shown in Table I and Fig. 2 respectively. The robot simulation and workpiece simulation models were built using the Robotics Toolbox for Matlab^{TM}[8], as can be seen in Fig. 3.

For a 6-Degree-of-Freedom robot, the location and orientation of end flange in the base coordinate system is defined by

$$A = A_1 A_2 A_3 A_4 A_5 A_6. \tag{1}$$

As shown in Fig. 1, the homogeneous transformation matrix A_7 which describes the position and orientation of the tool center point frame relative to the end flange flame is given by

$$A_7 = \begin{bmatrix} 1 & 0 & 0 & x \\ 0 & 1 & 0 & y \\ 0 & 0 & 1 & z \\ 0 & 0 & 0 & 1 \end{bmatrix}, \tag{2}$$

where x, y, z depend on the dimension of the end-effector having unit "m."

https://doi.org/10.1017/S0263574714001313 Published online by Cambridge University Press

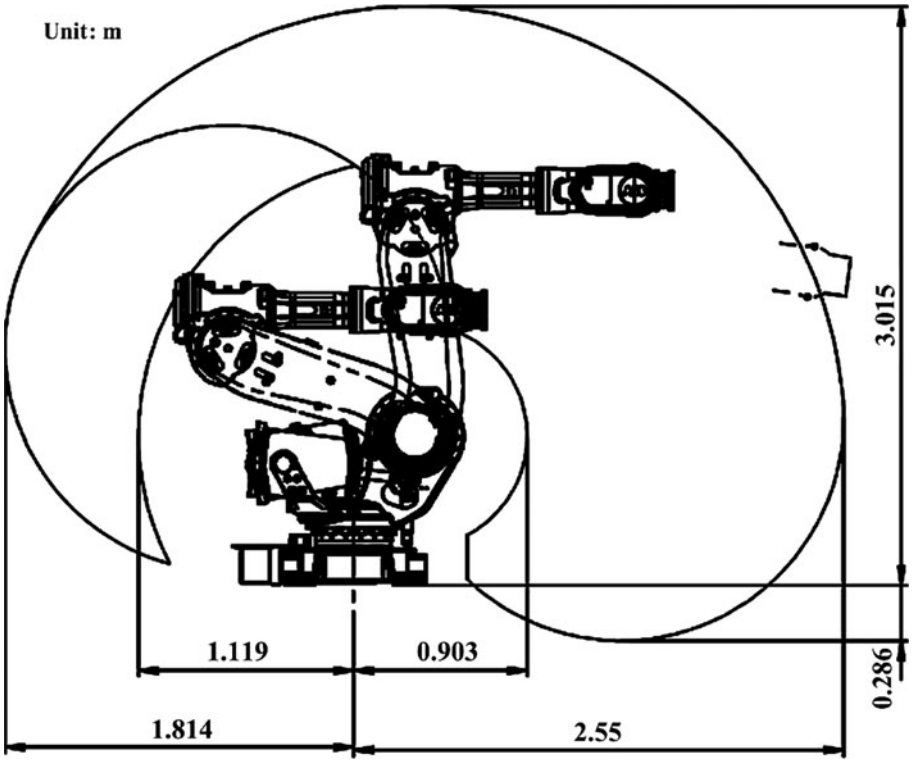


Fig. 2. Working range.

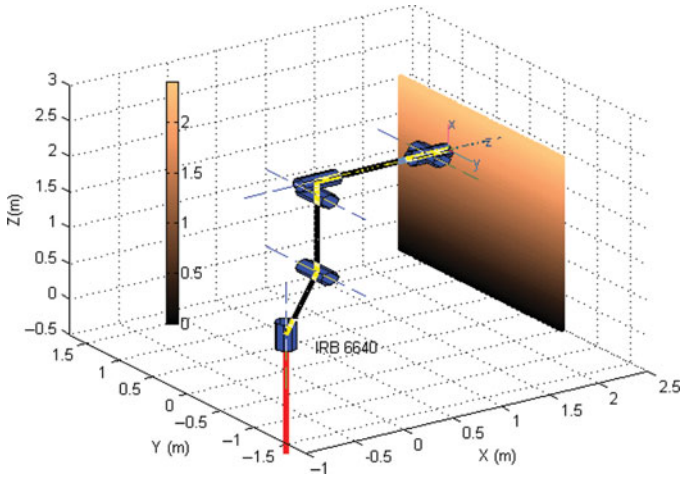


Fig. 3. The simulation model of robot and workpiece.

The translation vector is given by

$$p = (x \quad y \quad z). \tag{3}$$

The value of p is known according to the CAD model of the end-effector (shown in Fig. 4). For the pointing configuration,

$$p = (0.002 \quad 0 \quad 0.644). \tag{4}$$

For the hanging configuration,

$$p = (0.336 \quad 0 \quad 0.205). \tag{5}$$

https://doi.org/10.1017/S0263574714001313 Published online by Cambridge University Press

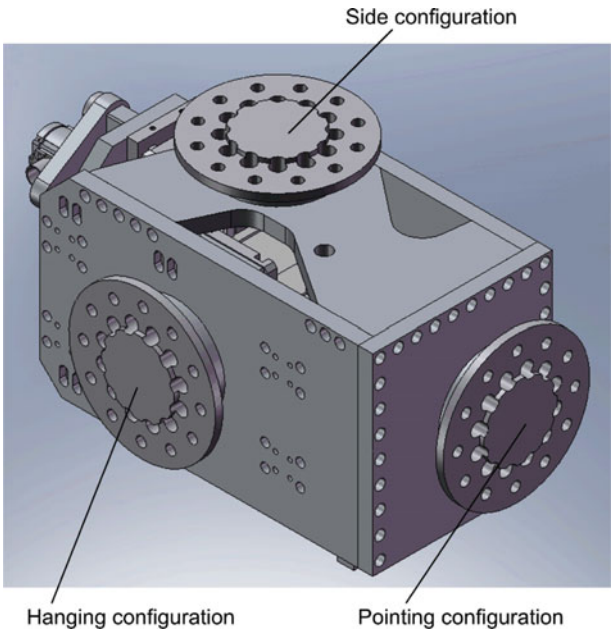


Fig. 4. The CAD model of end-effector.

For the side configuration

$$p = (-0.319 \quad -0.003 \quad 0.175). \tag{6}$$

It is assumed that there is only translation transformation between the base coordinate system and the workpiece coordinate system, and the position of a target point of the workpiece in the base coordinate system can be expressed as

$$P_B = (a \quad b \quad c(n)), \tag{7}$$

where a, b, and $c(n)$ are the X-, Y-, and Z-values in the base coordinate system (shown in Fig. 3) respectively,

$$c(n) = c_1 + (n-1)d, \tag{8}$$

where c_1 is the Z-value of the initial target point, n is the sequence number of target points in each column ($n = 1\ 101$), and d is the distance of the adjacent target point ($d = 0.022$ m).

In the drilling process, the axis of a drill bit should be perpendicular to the surface of the workpiece. In other words, the orientation of a tool coordinate system should be considered in each target point. There are two different motion transformations to achieve the requirement of position and orientation of the axis of a drill bit at each target point: one is from the workpiece coordinate system to the base coordinate system, and the other is from the tool coordinate system to the base coordinate system. Therefore, the expression for describing the relationship between two different motion transformations can be written as

$$A_1A_2A_3A_4A_5A_6A_7 = AA_7 = A_0, \tag{9}$$

where A_0 is the homogeneous transformation matrix from the workpiece coordinate system to the base coordinate system. For the pointing configuration,

$$A_0 = \begin{bmatrix} 0 & 0 & 1 & a \\ 0 & -1 & 0 & b \\ 1 & 0 & 0 & c(n) \\ 0 & 0 & 0 & 1 \end{bmatrix}. \tag{10}$$

https://doi.org/10.1017/S0263574714001313 Published online by Cambridge University Press

For the hanging configuration,

$$A_0 = \begin{bmatrix} 1 & 0 & 0 & a \\ 0 & -1 & 0 & b \\ 0 & 0 & -1 & c(n) \\ 0 & 0 & 0 & 1 \end{bmatrix}. \tag{11}$$

For the side configuration,

$$A_0 = \begin{bmatrix} -1 & 0 & 0 & a \\ 0 & 0 & -1 & b \\ 0 & -1 & 0 & c(n) \\ 0 & 0 & 0 & 1 \end{bmatrix}. \tag{12}$$

The homogeneous transformation matrices A_0 and A_7 are known, and the homogeneous transformation matrix A can be given by

$$A = A_0 A_7^{-1}. \tag{13}$$

Through Eq. (13), the joint values of the robot can be calculated.

Vector P_B is the location of the robot due to the existence of a linear guide, so the value of b can be taken as 0. Considering the workpiece size and the robot working range, the value of c_1 can also be taken as 0, i.e., the Z-value of the initial target point is 0 in the robot base coordinate system. Here, the only variable parameter in the vector P_B is a. The optimal value of a should be found for different mounted configurations. From the previous research,[9] the value of a can be taken as 2.8 m, 2.0 m, and 2.4 m for pointing, hanging, and side configurations respectively.

3. Effect of Mounted Configuration

3.1. Analysis of reachability

The methods of determining robot reachability include geometrical methods, closed form workspace methods, and inverse kinematics. The inverse kinematics is widely used in industrial applications, since serial industrial robot can be decoupled and solved analytically. If the joint angle can be computed for one target point along the end-effector path using Eq. (13), then the target point is reachable.

The reachability comparison for three mounted configurations can be seen in Fig. 5. The measurement of reachability is given by

$$r = m/t, \tag{14}$$

where m is the number of target points that can be reached under appropriate orientation, and t is the total number of target points. The value of r is 0.96, 0.87, and 0.85 for pointing, hanging, and side configurations respectively.

3.2. Analysis of manipulability

The manipulability measure proposed by Yoshikawa[10] was used to describe the kinematic ability of a robot in this study. Yoshikawa defined the measure of manipulability as

$$w = \sqrt{\det(J J^T)}, \tag{15}$$

where J is the Jacobian matrix. Here, the calculation of manipulability will be limited in the range of the 21st target point to the 96th target point because these target points are reachable for three mounted configurations. The effect of different mounted configurations on manipulability can be seen in Fig. 6. The side configuration is propitious to enhance the dexterity of the robotic drilling system, and the value can be kept consistent in a larger scope. The manipulability of the hanging configuration is affected by the location of target points, and there is a good manipulability in the middle area. The

https://doi.org/10.1017/S0263574714001313 Published online by Cambridge University Press

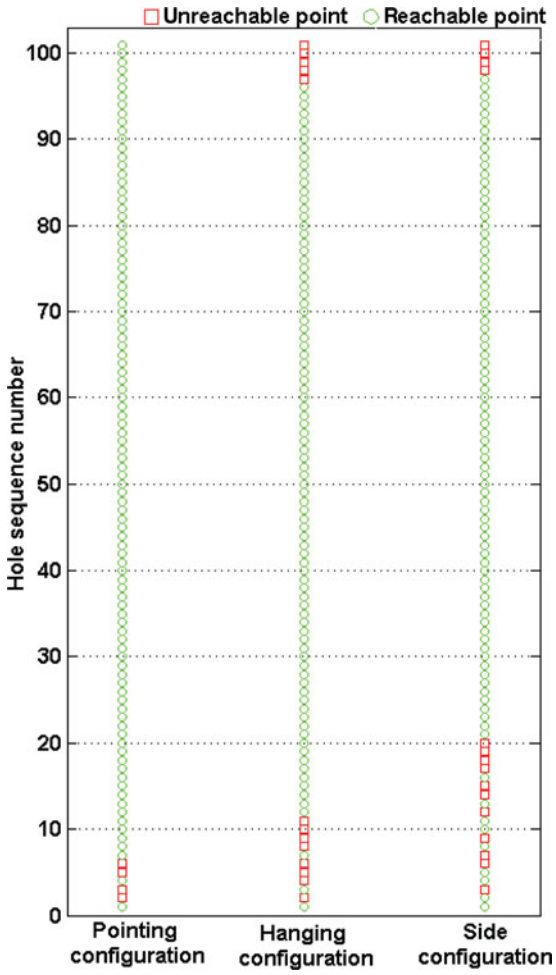


Fig. 5. The reachability comparison.

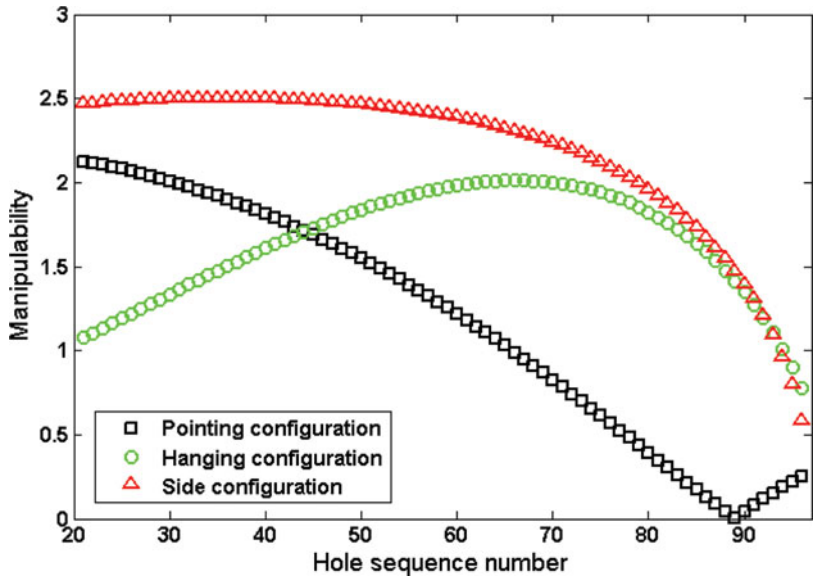


Fig. 6. The manipulability comparison.

https://doi.org/10.1017/S0263574714001313 Published online by Cambridge University Press

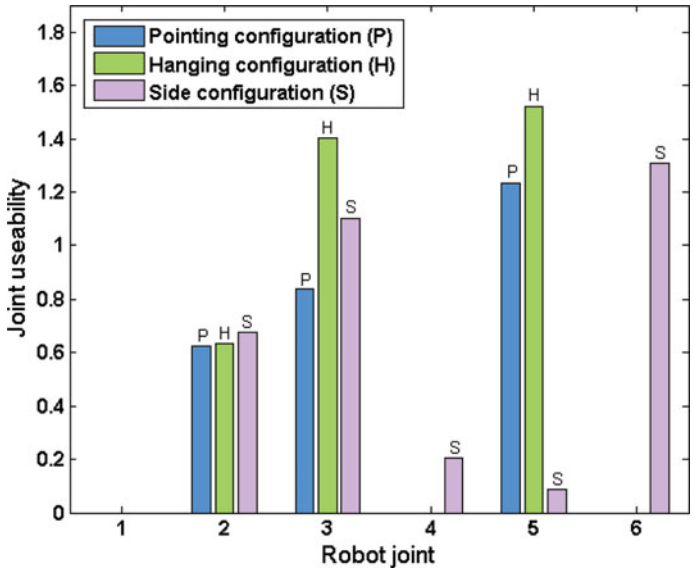


Fig. 7. The joint useability comparison.

locations of target points have a great effect on the manipulability of the pointing configuration, but manipulability as a whole is not good, which can be attributed to the axis of the drill bit and the axis of the sixth joint being coaxial.

3.3. Analysis of joint useability

When the end-effector moves from one target point to another in Cartesian space, the joints of a robot will produce angle changing in the joint space. After the tool center point passes through all target points, if both the sum of angular varieties for one joint and the sum of angular varieties for all joints are small, this will be beneficial to minimize the wear of robot's mechanical parts as well as energy consumption. Here the calculation of joint useability will also be limited in the range of the 21st target point to the 96th point.

When the end-effector moves from the ith target point to the $(i+1)$th target point, the angle variety of each joint is defined by

$$\Delta q_{ji}, \ \ j = 1 \cdots 6, \quad i = 21 \cdots 96, \tag{16}$$

and the sum of angular varieties for one joint is given by

$$q_j = \sum_{i=21}^{96} \left| \Delta q_{ji} \right|, \quad j = 1 \cdots 6. \tag{17}$$

The q_j is the measure of joint useability, and the lower value is better. Figure 7 presents the comparison of joint useability for different mounted configurations. The side configuration can make motion in Cartesian space translate into more joint motion in joint space. The point configuration can reduce the task's time, and increase productivity. In addition, for the pointing configuration,

$$\sum_{j=1}^{6} q_j = 2.69. \tag{18}$$

For the hanging configuration,

$$\sum_{j=1}^{6} q_j = 3.56. \tag{19}$$

https://doi.org/10.1017/S0263574714001313 Published online by Cambridge University Press

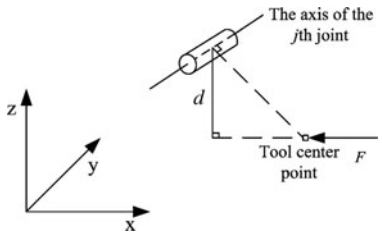


Fig. 8. The sketch map for calculating passive torque.

For the side configuration,

$$\sum_{j=1}^{6} q_j = 3.38. \tag{20}$$

In conclusion, the pointing configuration has higher productivity, lower energy consumption, and lower mechanical part wear compared with other configurations for flat workpiece.

3.4. Analysis of joint passive torque

The working manner of the end-effector induces joint passive torque. When the tool center point reaches a target point, the pressure foot of the end-effector will provide one-side mechanical pressure to the surface of the workpiece when drilling holes. The design of clamp force coupled with thrust force at pressure foot axis, and force of pressure foot axis will change with the thrust force. However, the force acting on robot's tool flange is constant, and its value equals the clamp force. This design makes the robot avoid bearing a dynamic load, but the static clamp force will produce passive torque on each joint of the robot. The deflection angle of each joint of robot is proportional to the passive torque. This deflection will change the position and orientation of the drill bit, thus causing poor hole quality. The sketch map of calculating passive torque can be seen in Fig. 8, and the passive torque is expressed as

$$M_j = F^* d, \quad j = 1 \cdots 6, \tag{21}$$

where F is the clamp force, and d is the force arm. Here, we select the fifth joint and the third joint of robot as analytical objects because the two joints are easier to be influenced by passive torque compared with other joints.

The passive torques of the fifth joint and the third joint for different configurations are shown in Figs. 9 and 10 respectively. The pointing configuration has the smallest passive torque on robot's fifth joint, and the passive torque can be eliminated by optimizing the dimension of the end-effector. For hanging and side configurations, the passive torque can be minimized by optimizing the dimension of the end-effector, but it can not be eliminated. The passive torque on the third joint of the robot has a consistent changing trend for all configurations. In general, the pointing configuration has a good exhibition for minimizing passive torque.

4. The Experiment

The workpiece has a flat surface and the TA15 titanium alloy is regarded as extremely difficult to cut materials, so the stiffness of robot is more important than the dexterity. Therefore, from the above analysis, the pointing configuration is a better choice for this application.

The testing of the robotic drilling system is shown in Fig. 11. Using plug gauge is a quick method to measure hole tolerance according to the go/no-go concept, so the hole tolerance was measured using the plug gauge. The measuring results showed that the hole tolerance accorded with H9 grade.

According to ISO9283 standard,[11] the position accuracy of an industrial robot is defined as:

$$AP_p = \sqrt{(\bar{x} - x_c)^2 + (\bar{y} - y_c)^2 + (\bar{z} - z_c)^2}, \tag{22}$$

where (x_c, y_c, z_c) is the commanded position, and $(\bar{x}, \bar{y}, \bar{z})$ is the mean attained position.

https://doi.org/10.1017/S0263574714001313 Published online by Cambridge University Press

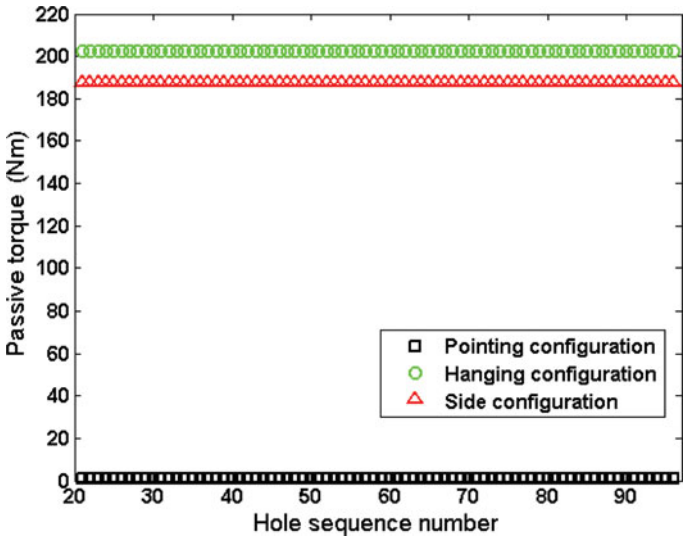


Fig. 9. The passive torques of the fifth joint comparison.

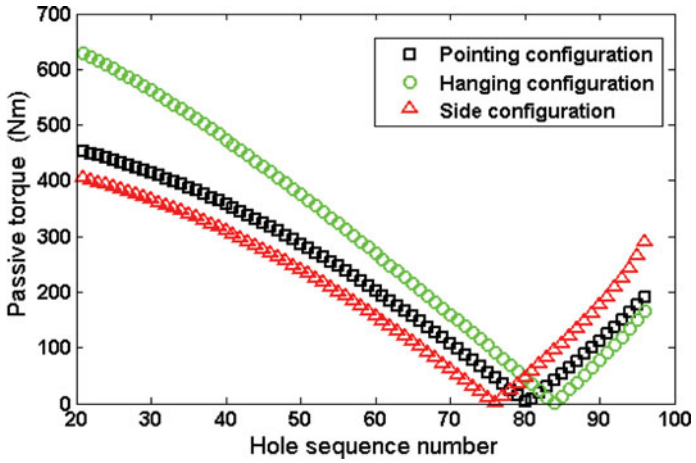


Fig. 10. The passive torques of the third joint comparison.

The hole position accuracy is measured by means of a laser tracker. By using the collected data for each of testing target points and Eq. (22), the calculated position accuracy for testing target points was within the required tolerance of 0.3 mm.

5. Conclusions

The advantages of the pointing configuration are good reachability, high productivity, low energy consumption, and low mechanical wear. At the same time, it can eliminate passive torque on the fifth joint of the robot. If the robot is equipped with some external motion unit, this mounting configuration is very fit for drilling holes in flat workpiece.

The hanging and side configurations improve robot's manipulability. However, the fifth joint of robot will bear passive torque, which can influence hole quality, especially for difficult-to-cut materials. If the robot drilling system integrates with relocating technology, the two mounting configurations are very suitable for drilling in a curved surface. The hanging configuration is more suitable for the situation having much yawing motion, and the side configuration is more suitable for the situation having much pitching motion.

https://doi.org/10.1017/S0263574714001313 Published online by Cambridge University Press

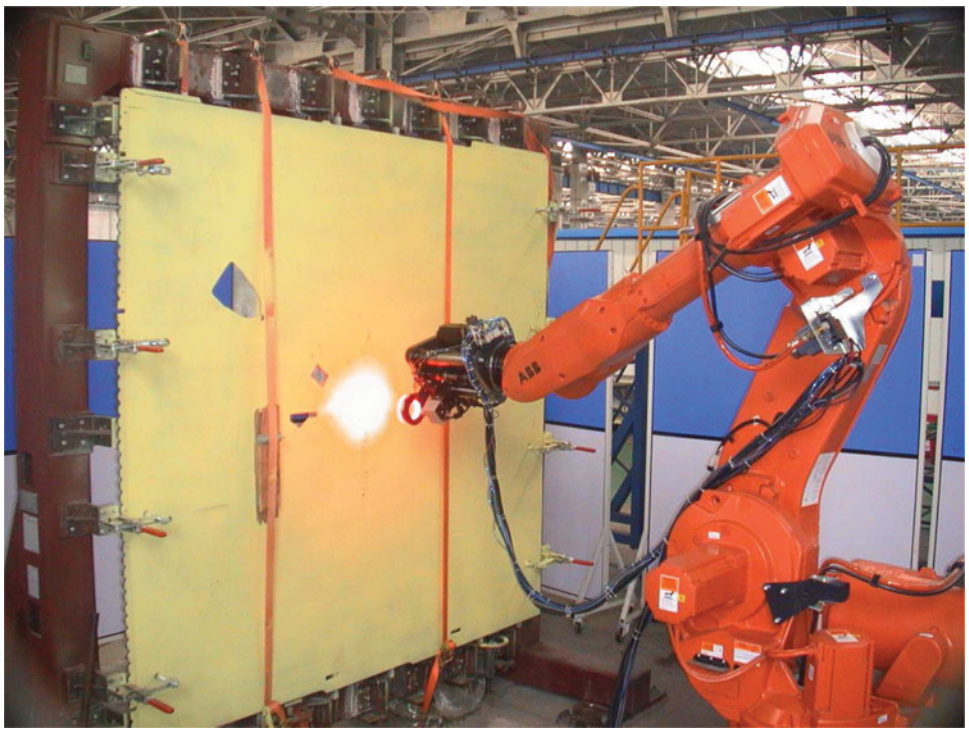


Fig. 11. The testing of the robotic drilling system.

Acknowledgements

This work was supported by the Project of International Science and Technology Cooperation of Department of Science and Technology of Henan Province of China (134300510046).

References

1. R. DeVlieg, K. Sitton, E. Feikert and J. Inman, "ONCE (One Sided Cell End Effector) Robotic Drilling System," *SAE 2002 Automated Fastening Conference & Exposition*, Chester, England. SAE Technical Papers 2002-01-2626.
2. J. Atkinson, J. Hartmann, S. Jones and P. Gleeson, "Robotic Drilling System for 737 Aileron," *SAE 2007 AeroTech Congress & Exhibition*, Los Angeles, CA. SAE Technical Papers 2007-01-3821.
3. R. Devlieg, "Robotic Trailing Edge Flap Drilling System," SAE 2009 *AeroTech Congress & Exhibition, Automated Fastening/Assembly & Tooling (AeroFast) – Automated Robotic Drill and Fastening Systems* Seattle, WA. SAE Technical Papers 2009-01-3244.
4. R. DeVlieg and E. Feikert, "One-Up Assembly with Robots," *SAE 2008 Aerospace Manufacturing and Automated Fastening Conference & Exhibition*, North Charleston, SC. SAE Technical Papers 2008-01-2297.
5. S. S. Bi and J. Liang, "Robotic drilling system for titanium structures," *Int. J. Adv. Manuf. Technol.* **54**, 767–774 (2011).
6. P. Webb, S. Eastwood and N. Jayaweera, "Automated aerostructure assembly," *Ind. Robot* **32**, 383–387 (2005).
7. J. Liang and S. S. Bi, "Design and experimental study of an end-effector for robotic drilling," *Int. J. Adv. Manuf. Technol.* **50**, 399–407 (2010).
8. P. I. A. Corke, "Robotics toolbox for matlab," *IEEE J. Robot. Autom.* **3**, 24–32 (1996).
9. J. Liang, Development of an End-Effector for Robotic Drilling and a Study on the Drilling of Titanium and Aluminium Stacks *Thesis*, Beijing University of Aeronautics and Astronautics, Beijing, China (2010).
10. T. Yoshikawa, "Manipulability of robotic mechanisms," *Int. J. Robot. Res.* **4**, 3–9 (1985).
11. J. Jack and H. Ray, "Measuring robot repeatability an application of ISO and ANSI standards," *Adv. Robot.* **10**, 503–520 (1995).

https://doi.org/10.1017/S0263574714001313 Published online by Cambridge University Press